Article

Theoretical Study for Adsorption−Diffusion on H-MOR and Pyridine Pre-adsorbed H-MOR of Dimethyl Ether Carbonylation

Jiabao Zhao, Weixin Qian, Hongfang Ma, Weiyong Ying, Peiqing Yuan, and Haitao Zhang*
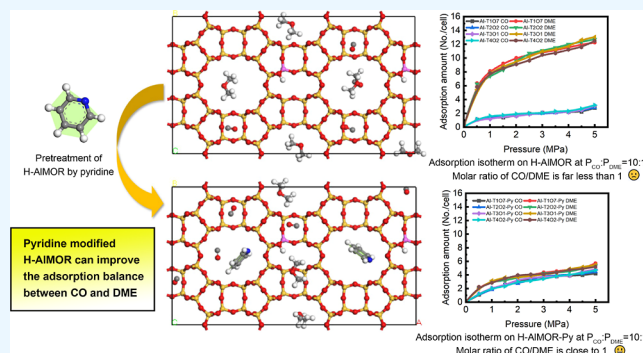
Read Online

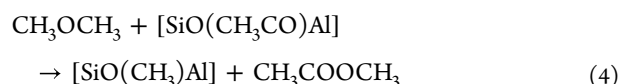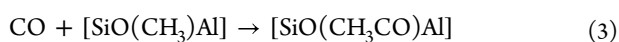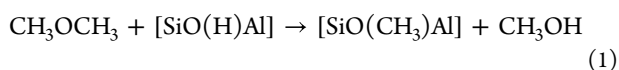| ACCESS | Metrics & More | Article Recommendations | SI Supporting Information |

ABSTRACT: For dimethyl ether (DME) carbonylation, pyridine pre-adsorbed hydrogen mordenite (H-MOR) is beneficial to prolonging the catalyst life. The adsorption and diffusion behaviors on periodic models H-AlMOR and H-AlMOR-Py were simulated. The simulation was based on Monte Carlo and molecular dynamics. The following conclusions were drawn from the simulation results. The adsorption stability of CO in 8-MR is increased, and the adsorption density of CO in 8-MR is more concentrated on H-AlMOR-Py. 8-MR is the main active site for DME carbonylation, so the introduction of pyridine would be beneficial for the main reaction. The adsorption distributions of methyl acetate (MA) (in 12-MR) and H_2O on H-AlMOR-Py are significantly decreased. It means the product MA and the byproduct H_2O are more easily desorbed on H-AlMOR-Py. For the mixed feed of DME carbonylation, the feed ratio (P_{CO}/P_{DME}) must reach 50:1 on H-AlMOR so that the reaction molar ratio can reach the theoretical value ($N_{CO}/N_{DME} \approx 1:1$), while the feed ratio on H-AlMOR-Py is only up to 10:1. Thus, the feed ratio can be adjusted, and raw materials can reduce consumption. In conclusion, H-AlMOR-Py can improve the adsorption equilibrium of reactants CO and DME and increase the concentration of CO in 8-MR.

Pretreatment of H-AlMOR by pyridine

Pyridine modified H-AlMOR can improve the adsorption balance between CO and DME

Adsorption isotherm on H-AlMOR at P_{CO}:P_{DME}=10:1 Molar ratio of CO/DME is far less than 1

Adsorption isotherm on H-AlMOR-Py at P_{CO}:P_{DME}=10:1 Molar ratio of CO/DME is close to 1

1. INTRODUCTION

Producing methyl acetate (MA) from CO and dimethyl ether (DME) is a key step of ethanol synthesis.[1−3] There are a lot of recent studies on how to improve the DME carbonylation reaction efficiency.[4,5] Cheung et al.[6] first reported that mordenite (MOR) and ferrierite (FER) with eight-membered ring pore (8-MR) structures have the highest yield. Bhan et al.[7,8] reported that the rate of MA production was linearly related to the number of Brønsted acid centers in the channels of 8-MR. The reaction mechanism was verified by He et al.[9] through continuous-flow ^{13}C NMR spectroscopy. Boronat et al.[10,11] concluded that the T3-O33 site in the 8-MR channel of MOR has a specific spatial domain-limiting effect on the CO insertion reaction, and other side reactions are hindered in this space. The reaction process is shown in eqs 1−4. Cai et al.[12] concluded that stronger acidity in the 8-MR site speeds up the formation rate of MA. Based on this, Boronat et al.[10] proposed that the insertion of CO into methoxy to form an acetyl group is the controlling step.

$$CH_3OCH_3 + [SiO(H)Al] \rightarrow [SiO(CH_3)Al] + CH_3OH \quad (1)$$

$$CH_3OH + [SiO(H)Al] \rightarrow [SiO(CH_3)Al] + H_2O \quad (2)$$

$$CO + [SiO(CH_3)Al] \rightarrow [SiO(CH_3CO)Al] \quad (3)$$

$$CH_3OCH_3 + [SiO(CH_3CO)Al]$$
$$\rightarrow [SiO(CH_3)Al] + CH_3COOCH_3 \quad (4)$$

According to Bao et al.,[9] the surface acetyl intermediates on H-MOR zeolites (CH_3CO-Z) were detected during DME carbonylation using in situ continuous-flow ^{13}C MAS NMR spectroscopy. The ex situ experiments show that the carbonyl peak of MA in the 8-MR channels appeared before the carbonyl signal from the 12-MR channels, indicating that the carbonylation reaction likely takes place within the narrow 8-MR channels, while the broader 12-MR channels provide a channel for the transport of reactants and products. The conclusion is consistent with that of Corma et al.[10,11] obtained from density functional theory calculations.

Although H-MOR has good selectivity, its catalyst life is short. Boronat et al.[10] found that H_2O leads to the formation of methanol and the reduction of the synthesis rate of MA.[13] Liu et al.[14] put forward a similar conclusion. Therefore, it is
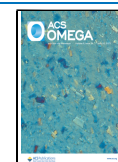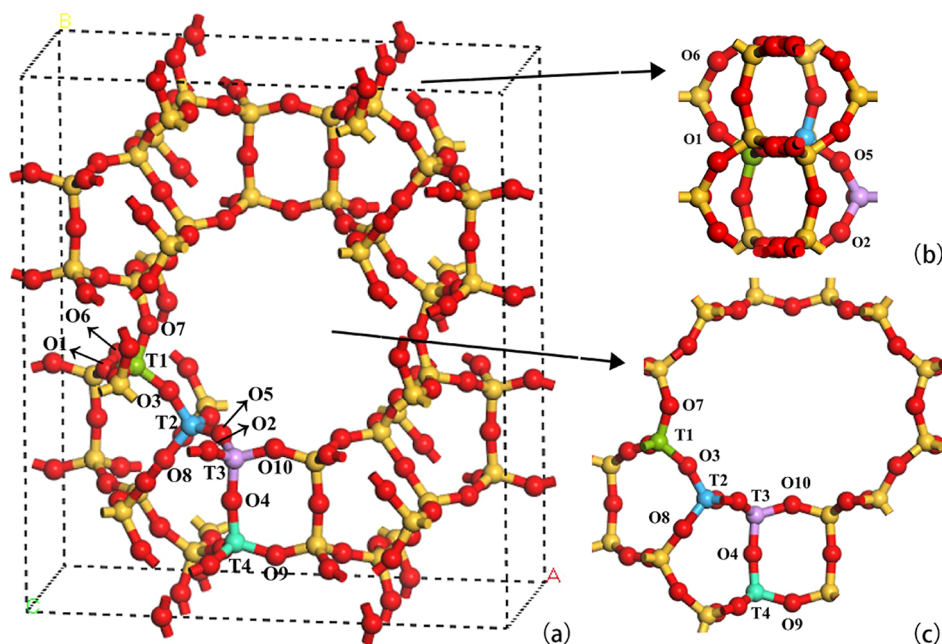
Figure 1. (a) Schematic diagram of different active sites on the H-MOR model along the [0 0 1] direction. (Color scheme: O, red; Si, yellow) (b) partially enlarged diagram of the channel along the [0 0 1] direction (c) partially enlarged diagram of the channel along the [1 0 0] direction.

crucial for the removal of the byproduct H_2O. In addition, Rasmussen et al.[15] and Chen et al.[16,17] confirmed that ketene intermediates are formed by the insertion of CO molecules into methoxy groups to form an activated complex acetyl group. Coke and larger carbon structures are formed, so the catalyst is deactivated. Zhao et al. found[18] that the Brønsted acidic site of the twelve-membered ring (12-MR) in H-MOR is the main factor of carbon accumulation.

The rapid deactivation caused by coke formation in 12-MR is considered a primary constraint for its commercial application.[19] To solve the above problems, Liu et al.[14] found that pyridine adsorption can enhance the stability of H-MOR, with the product MA yielding over 30%. The process works as follows. Adsorbed pyridine preferentially passivated the acidic sites in the 12-MR pores of H-MOR but could not access the acidic sites in the 8-MR pores. Thus, DME carbonylation was directed to occur mainly in the 8-MR pores of the H-MOR-Py catalyst, which led to the effective inhibition of coke formation and superior catalytic stability.[14] Pre-adsorption of pyridine on H-MOR improved its catalytic stability for DME carbonylation to MA.

However, the 12-MR of H-MOR is clogged with pyridine, which has a certain impact on the channel structure. The adsorption and diffusion properties of H-MOR will be changed after the pretreatment of pyridine. Few reports have reported the effect of pyridine pre-adsorption on the mass transfer of H-MOR. Thus, this paper will build H-AlMOR and H-AlMOR-Py models. The adsorption and diffusion properties of the DME carbonylation system were calculated and studied on the model. The simulation is based on Monte Carlo and molecular dynamics simulations. The effect of pyridine modification on DME carbonylation is explored. The result plays a guiding role in the modification and optimization of H-MOR.

2. ADSORPTION–DIFFUSION MODEL ESTABLISHMENT AND VERIFICATION

2.1. Adsorption–Diffusion Model Establishment. As shown in Figure 1, the structure of MOR was developed.[20−22] It is mainly composed of the twelve-membered ring (12-MR) along the [0 0 1] direction with a size of 6.5×7.0 Å^2 and the eight-membered ring (8-MR) along the [0 1 0] direction with a size of 2.6×5.7 Å^2. They are elliptical and intersect vertically.[4,20−22] The original structure of MOR was obtained initially from the database of the International Zeolite Association (IZA) official website. The parameters of MOR are $18.26 \times 20.53 \times 7.54$ Å^3 and $\alpha = \beta = \gamma = 90°$. Liu et al.[23] reported that the periodic model was used to obtain the properties of H-MOR because the gas diffuses inside and outside the surface.

Considering the computing power of the server and the accuracy of the simulation, the H-AlMOR $(2 \times 1 \times 1)$ bimolecular model was chosen as the base model, as Figure 2a shows, and the size of which is $36.52 \times 20.53 \times 7.54$ Å^3. The silica–alumina ratio of H-AlMOR was chosen to be 9−15. There are four different tetrahedral sites in the backbone of H-MOR, usually Si or Al atoms. As shown in Figure 1, this paper defines 10 different O atomic sites as O1 to O10 sites.
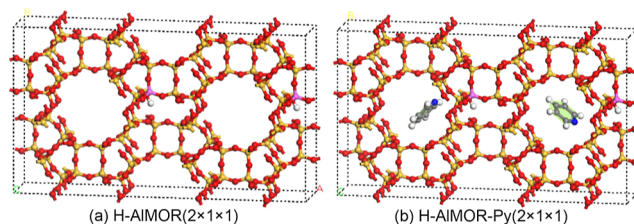

Figure 2. Schematic diagram of the adsorption–diffusion model along the [0 0 1] direction (taking Al-T3O1 and Al-T3O1-Py as examples. Color scheme: O, red; Si, yellow; Al, pink; C, gray; H, white; N, blue).
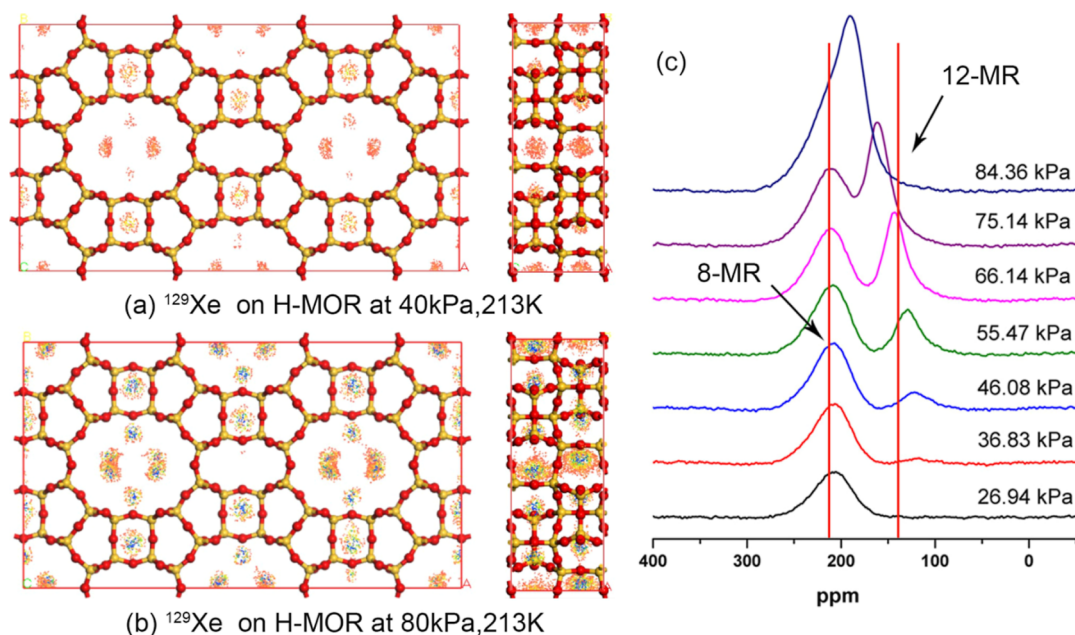
Figure 3. Adsorption verification: (a) ^{129}Xe adsorption density map on H-MOR at 40 kPa, 213 K; (b) ^{129}Xe adsorption density map on H-MOR at 80 kPa, 213 K; (c) NMR spectra of ^{129}Xe.

Chibani[24] et al. reported that the structure is most stable when the Al atom is located at T1, and the equilibrium proton is at O7. When the Al atom is located at T2, T3, and T4, the equilibrium proton is, respectively, at O2, O1, and O2. These four molecular models are defined as Al-T1O7, Al-T2O2, Al-T3O1, and Al-T4O2. Figure 2a is the model of H-AlMOR (2 × 1 × 1) (taking Al-T3O1 as an example).

Based on the model, this paper introduces two pyridine molecules into each of the above models. Pyridine is introduced into H-AlMOR zeolite by adsorption. The introduction of pyridine does not change the properties of the H-AlMOR. There are also four types of models defined as Al-T1O7-Py, Al-T2O2-Py, Al-T3O1-Py, and Al-T4O2-Py. Figure 2b is the model of H-AlMOR-Py (2 × 1 × 1) (taking Al-T3O1-Py as an example). According to Liu's[4] article, the pre-adsorption of pyridine on H-AlMOR led to preferential blocking of the acidic sites in 12-MR pores while leaving the acidic sites in 8-MR pores undisturbed. The same conclusion is obtained by the simulation method. Due to the large size of the pyridine molecule, it can only be located in 12-MR but cannot pass through 8-MR, as shown in Figure 2b.

The simulation was executed by Materials Studio software. The adsorption simulation was performed by the Sorption module based on the Monte Carlo method and random sampling.[22,25−28] This paper used the Metropolis method. 1 × 10^6 Monte Carlo steps were required in the whole process, which include 1 × 10^5 equilibrium steps and 9 × 10^5 production steps. COMPASS II was chosen for the system force field.[29,30] It is optimized based on the COMPASS force field, which makes the simulation data closer to the experimental data. The Ewald and Group method was selected as 1 × 10$^{−4}$ kcal/mol. Atom-based was set as the van der Waals force. The cut-off distance was set to 15.5 Å.[23,29−31] The cut-off distance is independent of model size in this system, and the description is listed in the Supporting Information.

The diffusion simulation was performed by the Forcite module. The *NVT* system was set up as a simulation environment, where the particle number, the system volume,

and the system temperature were fixed as constants. The Nosé method was set to control the system temperature. The coupling time was chosen as 1 ps. The COMPASS II force field was set. The Ewald method was set for electrostatic potential. The Verlet algorithm was chosen for velocity. The simulation started with an annealed state carried out for a total of 10 ns with a step of 1 fs.[23,32] Mean square displacement-simulation time (MSD-T) images were obtained from the results directly. The first 1 ns stable data was taken for analysis. Then, the self-diffusion coefficient (D_S) was calculated by Einstein's equation

$$D_S = \frac{1}{2n} \lim_{t \to \infty} \frac{d}{dt} \langle |r(t) - r(0)|^2 \rangle \tag{5}$$

In eq 5, D_S denotes the self-diffusion coefficient, and $|r(t) - r(0)|^2$ denotes mean square displacement (MSD).

2.2. Adsorption−Diffusion Model Verification. By referring to relevant literature, there is no adsorption and diffusion data directly related to DME carbonylation over H-MOR. So the article simulated the adsorption properties of ^{129}Xe and the diffusion properties of CH_4 on H-MOR compared with the experimental data to verify the dependability of the model.[33] The adsorption properties are shown in Figure 3. When the pressure is at 40 kPa (low pressure), ^{129}Xe atoms tend to be adsorbed on 8-MR. But under 80 kPa (high pressure), atoms are uniformly distributed on 12-MR and 8-MR. The conclusion is consistent with the NMR experimental results of He.[33] Figure 4 shows the MSD-T image, which is obtained from the simulation. The self-diffusion coefficient of CH_4 on H-MOR can be calculated by the MSD-T image, which is $4.07 × 10^{−9}$ m^2/s. The PFG-NMR experimental results of CH_4 were $3.7 × 10^{−9}$ m^2/s. By comparing the simulation data with the experimental data, the reliability of the model can be proven.

3. RESULTS AND DISCUSSION

Cheung et al.[6] showed that the DME carbonylation reaction was carried out at 423−493 K, 0.15−2.50 MPa. Zhou et al.[34]
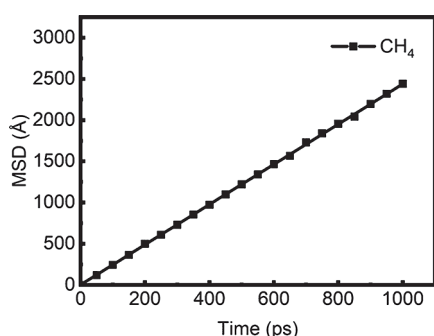
Figure 4. Diffusion verification: MSD-T image of CH_4 on H-MOR.

found that when the temperature was above 433 K, chemisorption formation on Brønsted acid centers was observed by in situ DRIFT. Thus, this paper set the reaction condition as 433 K, 0.2 MPa. The gas molecule contains the reactants CO and DME, the product MA, and the byproduct H_2O. The adsorption and diffusion behavior of pure molecules on H-AlMOR and H-AlMOR-Py of the DME carbonylation was investigated. The adsorption performances of mixed gas molecules (CO and DME) at a certain feed ratio were also investigated.

3.1. Adsorption Properties of Pure Gas. *3.1.1. Adsorption Isotherm.* An adsorption isotherm is useful as a guide for the study and optimization of molecular adsorption performance. In this chapter, Langmuir adsorption isotherms of gas molecules at H-AlMOR and H-AlMOR-Py were simulated at 433 K. All the curves belong to the Langmuir I type curve, which is the main characteristic of porous materials of zeolite molecular sieves.

First, the adsorption isotherm trend of gas on H-AlMOR was analyzed, as shown in Figure 5. The curves of CO increased rapidly throughout the pressure range with no saturation trend. The curves of DME increased rapidly when the pressure was less than 1 MPa, while when the pressure was greater than 1 MPa, the adsorption amount remained almost constant. The curves of MA increased rapidly when the pressure was less than 1.5 MPa, and the rate slowed down
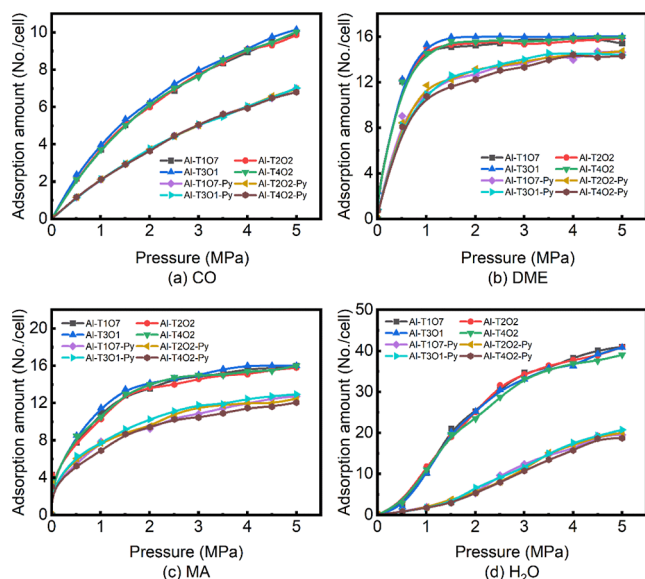

Figure 5. Adsorption isotherms of different pure gas molecules on H-AlMOR and H-AlMOR-Py at 433 K.

when the pressure was over 1.5 MPa. The curves of H_2O increased rapidly throughout the pressure range, which is similar to that for CO, but steeper. At the same condition, the adsorption of H_2O is about 3−4 times that of CO on H-AlMOR.

As Figure 5 shows, the variation trend of pure gases on H-AlMOR-Py with pressure is similar to that on H-AlMOR. But the adsorption amount on H-AlMOR-Py is slightly lower under the same pressure. The adsorption amount of different types of models (Al-T1O7−Al-T4O2 and Al-T1O7-Py−Al-T4O2-Py) is slightly different but in the same order of magnitude. Thus, this paper analyzed the average data. Generally, it is worth noting that the adsorption amount of CO, DME, and MA on Al-T3O1 is larger. The conclusion also applies to H-AlMOR-Py.

It is worth noting that the adsorption isotherms of the reactants CO and DME on H-AlMOR are quite different: CO adsorption amount increases rapidly over the whole pressure range; DME adsorption increases rapidly at low pressure but tends to be saturated at high pressure. DME molecule consists of two methyl groups, which can be hydrogen-bonded to the oxygen atom of the zeolite skeleton.[10] In contrast, CO molecules have only carbon−oxygen triple bonds, which can not be combined with the zeolite skeleton. Thus, under the same reaction conditions, the adsorption amount of CO is always insufficient for DME in carbonylation reaction. So, the reaction ratio depends to some extent on the amount of CO adsorbed.

The adsorption amount of gas molecules on H-AlMOR and H-AlMOR-Py at 433 K, 0.2 MPa is shown in Table 1. After

Table 1. Adsorption Amount (N_{ads}) of Pure Gas Molecules on H-AlMOR and H-AlMOR-Py at 433 K, 0.2 MPa (Unit: mol/mol)

molecular model	CO	DME	MA	H_2O
Al-T1O7	0.92	11.51	6.63	0.59
Al-T1O7-Py	0.71	5.15	3.35	0.26
Al-T2O2	0.91	11.52	7.36	0.53
Al-T2O2-Py	0.71	4.70	3.85	0.22
Al-T3O1	0.92	11.56	7.54	0.62
Al-T3O1-Py	0.72	5.15	4.91	0.33
Al-T4O2	0.92	11.26	7.00	0.54
Al-T4O2-Py	0.69	4.22	2.63	0.31
average N_{ads} on H-AlMOR	0.92	11.46	7.13	0.57
average N_{ads} on H-AlMOR-Py	0.71	4.80	3.68	0.28

pyridine modification, the adsorption amount of CO decreased by 22.83% (0.92 → 0.71 mol/mol), and that of DME decreased by 58.12% (11.46 → 4.80 mol/mol). The adsorption amount of product MA decreased by 48.39% (7.13 → 3.68 mol/mol), and that of H_2O decreased by 50.88% (0.57 → 0.28 mol/mol). The adsorption amount of CO decreased by only 22.83%, which had the smallest effect among all molecules. The decrease of DME is 2−3 times that of CO. According to Rasmussen et al.,[15] the theoretical consumption molar ratio of CO/DME in DME carbonylation is 1:1, which means that the introduction of pyridine will help balance the two main reactants in H-AlMOR. The amount of MA was greatly affected by pyridine pretreatment, which is conducive to the desorption of MA. In addition, H-AlMOR-Py can greatly reduce the adsorption amount of byproduct H_2O.
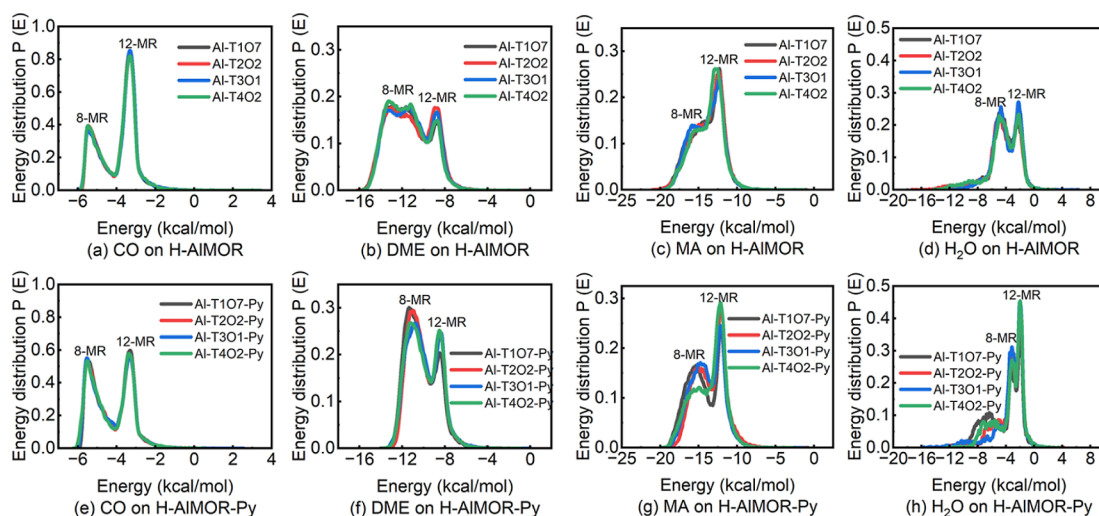
Figure 6. Adsorption energy distribution of pure gas molecules on H-AlMOR and H-AlMOR-Py at 433 K.

Table 2. Adsorption Energy (E_{ads}) of Pure Gas Molecules on H-AlMOR and H-AlMOR-Py at 433 K, 0.2 MPa (Unit: kcal/mol)

molecular model	CO		DME		MA		H_2O	
	8-MR	12-MR	8-MR	12-MR	8-MR	12-MR	8-MR	12-MR
Al-T1O7	−5.46	−3.32	−11.65	−8.85	−14.25	−12.25	−4.95	−2.35
Al-T1O7-Py	−5.45	−3.25	−11.35	−8.55	−15.25	−11.95	−3.15	−1.95
Al-T2O2	−5.45	−3.35	−11.65	−8.65	−14.45	−12.35	−4.95	−2.25
Al-T2O2-Py	−5.55	−3.35	−11.25	−8.45	−15.15	−12.05	−3.15	−1.95
Al-T3O1	−5.55	−3.35	−11.35	−8.75	−14.95	−12.25	−4.75	−2.25
Al-T3O1-Py	−5.55	−3.35	−10.85	−8.35	−15.05	−12.15	−3.15	−2.05
Al-T4O2	−5.55	−3.35	−11.65	−8.75	−14.65	−12.55	−4.95	−2.15
Al-T4O2-Py	−5.55	−3.35	−11.25	−8.55	−14.95	−12.15	−3.15	−2.05
average E_{ads} on H-AlMOR	−5.50	−3.34	−11.58	−8.75	−14.58	−12.35	−4.90	−2.25
average E_{ads} on H-AlMOR-Py	−5.53	−3.33	−11.18	−8.48	−15.10	−12.08	−3.15	−2.00

3.1.2. Adsorption Energy Distribution. Adsorption iso-therms can help us analyze the adsorption properties on a macro level. However, it cannot help us fully understand the adsorption properties on the internal channels. Thus, Figure 6 simulates the adsorption energy distribution curves of adsorbed molecules on H-AlMOR (Al-T1O7−Al-T4O2) and H-AlMOR-Py (Al-T1O7−Al-T4O2) at 433 K, 0.2 MPa. The adsorption energy peaks of 8-MR and 12-MR are listed in Table 2.

As shown in Figure 6a,e, there are two peaks in the image, which means that there are two potential adsorption zones for CO. After pyridine pretreatment, the adsorption energy of CO in 8-MR becomes stronger (−5.50 → −5.53 kcal/mol), and that in 12-MR becomes weaker (−3.34 → −3.33 kcal/mol). Bhan[7,8] et al. have experimentally determined that the 8-MR acts as the active center, and the rate of carbonylation increases linearly with CO pressure. It can be seen that the adsorption stability of CO on 8-MR is stronger, which means H-AlMOR-Py is favorable for CO adsorption and reaction. The adsorption energy of DME increased in 8-MR by 3.45% (−11.58 → −11.18 kcal/mol) and in 12-MR by 3.09% (−8.75 → −8.48 kcal/mol). It means that pyridine pretreatment can reduce the adsorption stability of DME. As shown in Figure 6b, the 8-MR peaks on H-AlMOR are wide, which is due to the high distribution density of DME on 8-MR. As can also be proven in Figure 7c, the adsorption density of DME on 8-MR is larger (the area of blue dots is large), which corresponds to the wider adsorption energy distribution of the 8-MR peak in

Figure 6b. According to Table 2, it can be seen that the adsorption energy of DME on 8-MR and 12-MR is always lower than that of CO, which means that DME has stronger adsorption stability than CO. Therefore, the feed of CO is always insufficient to DME.

As shown in Figure 6c,g, the adsorption energy for MA decreased by 3.57% (−14.58 → −15.10 kcal/mol) in 8-MR but increased by 2.19% (−12.35 → −12.08 kcal/mol) in 12-MR. MA is mainly distributed on 12-MR due to its larger molecular weight, and reduced adsorption energy means that the product is more easily desorbed. The adsorption energy for H_2O increases by 35.71% in 8-MR (−4.90 → −3.15 kcal/mol) and 11.11% in 12-MR (−2.25 → −2.00 kcal/mol). It indicates that H-AlMOR-Py was beneficial in reducing the byproduct adsorption stability, thus promoting the occurrence of the main reaction. As Figure 6h shows, H_2O formed a wide peak with an average adsorption energy range of −5.6 to −8.0 kcal/mol, which was analyzed due to the exothermic reaction of pyridine and water. Due to the small adsorption density, it has little influence on the overall analysis.

3.1.3. Adsorption Density Map. Analyzing the adsorption distributions in Figure 7, it can be found that the introduction of pyridine occupied the 12-MR. Therefore, the adsorption densities of 12-MR molecules all decreased, while the adsorption densities of molecules in 8-MR are different. Figure 7a,b shows a more concentrated adsorption density of CO in 8-MR after pyridine pre-adsorption. Studies by Bhan[7] et al. and Rasmussen[35] et al. showed that 8-MR was the main active site
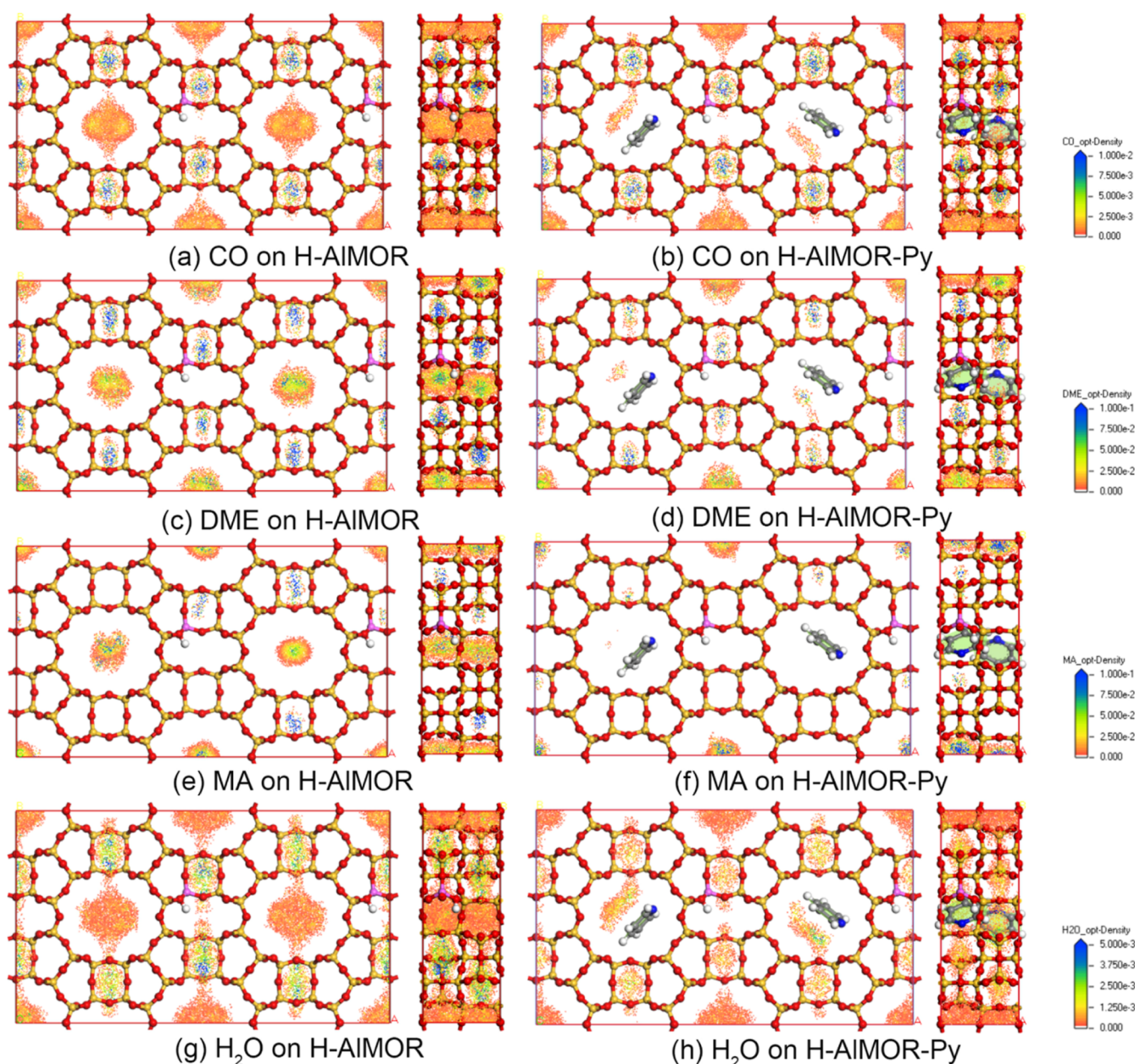
Figure 7. Adsorption density map for pure gas molecules on H-AlMOR and H-AlMOR-Py at 433 K, 0.2 MPa.

for DME carbonylation, so the introduction of pyridine would also increase the concentration of the reactant CO in the active site 8-MR. For DME, the adsorption was reduced in both 8-MR and 12-MR. For product MA, the introduction of pyridine caused a significant decrease in 12-MR within the molecular sieve, as can be seen in Figure 7e,f, which is conducive to the desorption of the product MA. For H$_2$O, the adsorption distribution across the entire molecule goes down, which is conducive to reducing the adsorption of the byproduct.

3.2. Diffusion Properties of Pure Gas. According to the research on adsorption properties, pyridine modification has a positive effect. But, the channel structure change caused by pyridine pretreatment will certainly affect the diffusion properties. This part continues to study the diffusion properties. Five gas molecules are introduced into each model to ensure that the amount is the same to compare with each other.

The MSD-T images are shown in Figure 8. Transformed by Einstein's equations, the self-diffusion coefficient is given in Table 3. According to Liu[14] et al., $D_S < 10^{-12}$ m^2/s is considered to be a slow expansion in the zeolite. The data in Table 3 are all in the range of 10^{-8} to 10^{-9}, which means that gas can spread freely. After pyridine treatment, the D_S of CO decreased by 36.54% ($2.53 \times 10^{-8} \rightarrow 1.60 \times 10^{-8}$ m^2/s) and that of DME decreased by 40.66% ($1.82 \times 10^{-8} \rightarrow 1.08 \times 10^{-8}$ m^2/s). The D_S of MA decreased by 75.79% ($1.27 \times 10^{-8} \rightarrow 3.10 \times 10^{-9}$ m^2/s), and that of H$_2$O decreased by 35.85% ($2.88 \times 10^{-8} \rightarrow 1.85 \times 10^{-8}$ m^2/s).

According to Figure 7, pyridine mainly occupies 12-MR because of its large molecular weight. For all molecules, when 12-MR is filled with pyridine, the D_S decreases to a large extent, which also means that 12-MR represents a mass transfer site for DME carbonylation. The result is consistent with the conclusion obtained by Liu[4] et al. Among them, H-AlMOR-Py has little effect on CO diffusion. CO and H$_2$O are
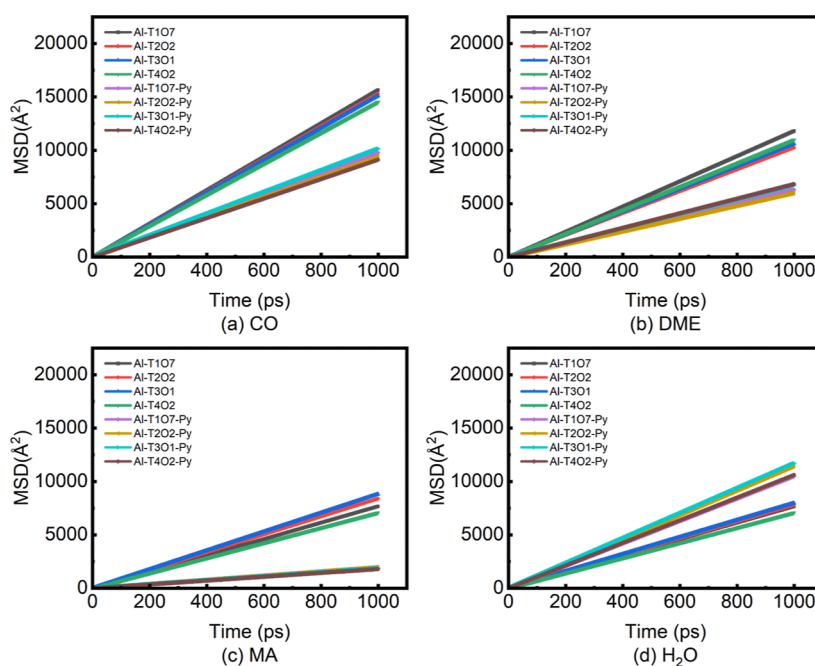
Figure 8. MSD-T image of pure gas molecules on H-AlMOR and H-AlMOR-Py at 433 K, 0.2 MPa.

Table 3. Self-diffusion Coefficient (D_S) of Pure Gas Molecules on H-AlMOR and H-AlMOR-Py at 433 K, 0.2 MPa (Unit: m²/s)

molecular model	CO	DME	MA	H_2O
Al-T1O7	2.61×10^{-8}	1.97×10^{-8}	1.28×10^{-8}	2.74×10^{-8}
Al-T1O7-Py	1.63×10^{-8}	1.05×10^{-8}	3.14×10^{-9}	1.75×10^{-8}
Al-T2O2	2.55×10^{-8}	1.71×10^{-8}	1.30×10^{-8}	2.83×10^{-8}
Al-T2O2-Py	1.57×10^{-8}	1.00×10^{-8}	3.26×10^{-9}	1.91×10^{-8}
Al-T3O1	2.52×10^{-8}	1.77×10^{-8}	1.33×10^{-8}	2.94×10^{-8}
Al-T3O1-Py	1.69×10^{-8}	1.12×10^{-8}	3.09×10^{-9}	1.95×10^{-8}
Al-T4O2	2.42×10^{-8}	1.83×10^{-8}	1.18×10^{-8}	3.02×10^{-8}
Al-T4O2-Py	1.52×10^{-8}	1.14×10^{-8}	3.00×10^{-9}	1.77×10^{-8}
average D_S of H-AlMOR	2.53×10^{-8}	1.82×10^{-8}	1.27×10^{-8}	2.88×10^{-8}
average D_S H-AlMOR-Py	1.60×10^{-8}	1.08×10^{-8}	3.10×10^{-9}	1.85×10^{-8}

small, the diffusion of which is more flexible and does not depend on the 12-MR. Thus, D_S of them has little effect. However, DME and MA are mainly distributed in 12-MR due to their larger molecular weight. The D_S of them is greatly affected. Thus, the diffusion performance of H-AlMOR-Py is worthy of optimization and improvement.

3.3. Adsorption Properties of Mixed Gas. *3.3.1. Adsorption Isotherm.* The above research is for pure gas. However, CO and DME usually enter the reactor as gaseous mixtures with a CO/DME molar ratio of 10:1−50:1[6,36] in the actual reaction. Thus, the adsorption isotherm of CO/DME mixtures with a feed ratio of 10:1, 20:1, and 50:1 (P_{CO}/P_{DME} = 10:1, 20:1, and 50:1) was simulated.

It can be seen from Figure 9 that the isotherms of CO and DME in the mixture are similar to those of pure gases but always less than pure gas. This may be due to the interaction between CO and DME, which prevents the adsorption of each other. As shown in Figure 9, with the increase of CO partial pressure, the adsorption amount of CO increases and the adsorption amount of DME decreases. Under the same conditions, the degree of molecular amount change in H-AlMOR-Py is more significant.

According to the mechanism proposed by Boronat[10] (eqs 1−4), we know that the molar ratio of CO/DME (N_{CO}/N_{DME})

is 1:1 for reaction. We also know that the adsorption stability of DME is always stronger than that of CO. Thus, the adsorption amount of DME is always more than that of CO from Chapter 3.1.1. Only by increasing the CO feeding amount can let N_{CO}/N_{DME} reach 1:1.

Table 4 shows the N_{CO}/N_{DME} adsorbed on H-AlMOR and H-AlMOR-Py at different feed ratios. Compared with N_{CO}/N_{DME} on H-AlMOR, that on H-AlMOR-Py increased 2.53 times (0.17 → 0.43 mol/mol) at P_{CO}/P_{DME} = 10:1, 2.06 times (0.31 → 0.64 mol/mol) at P_{CO}/P_{DME} = 20:1, and 1.86 times at P_{CO}/P_{DME} = 50:1 (0.76 → 1.41 mol/mol).

For H-AlMOR-Py, the optimal reaction P_{CO}/P_{DME} (N_{CO}/N_{DME} is equal to 1) was around 10:1. While for H-AlMOR, the P_{CO}/P_{DME} should be over 50:1. It can be seen that H-AlMOR-Py can adjust the N_{CO}/N_{DME} equal to 1:1 at a low feed ratio. The introduction of pyridine is conducive to the adsorption balance of the main reactants (CO and DME) in H-AlMOR.

3.3.2. Adsorption Density Map. The adsorption density distribution diagram of mixed gas feed is shown in Figure 10. As Figure 10a,b shows, it can be seen that the adsorption density in 8-MR is more concentrated, while that in 12-MR is greatly reduced after pyridine pre-adsorption. As Figure 10c,d shows, the adsorption density of DME in 12-MR and 8-MR both decreased. Cheung[6,36] reported that for DME carbon-
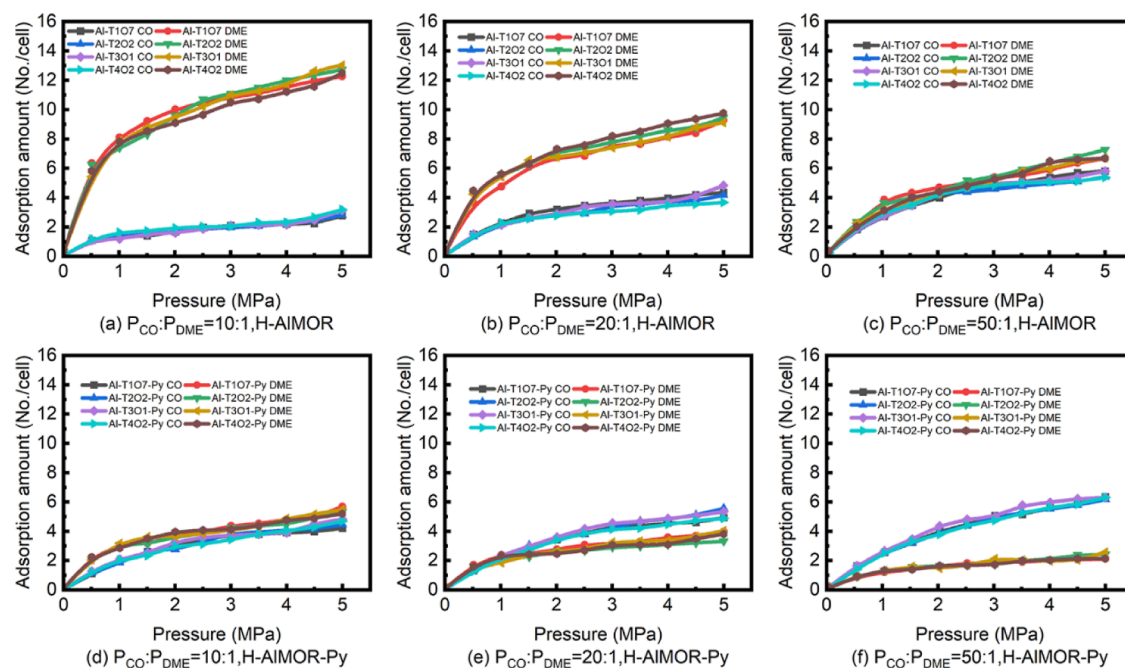
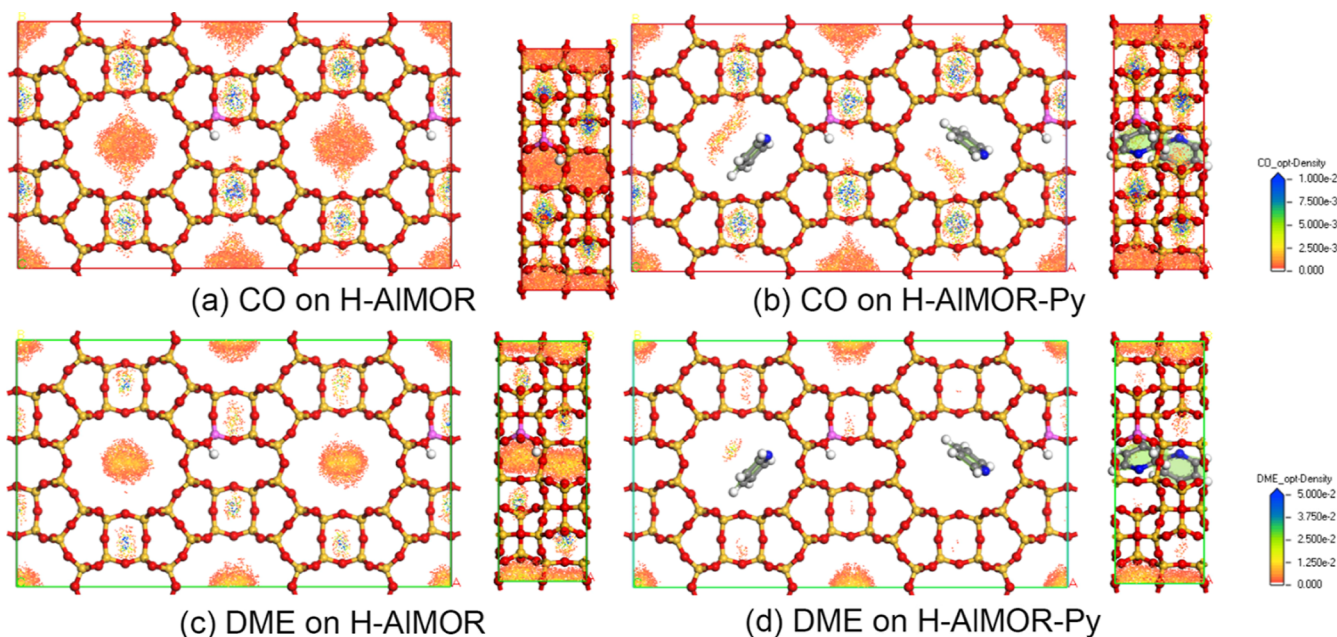**Figure 9.** Adsorption isotherms of CO and DME on H-AlMOR and H-AlMOR-Py at 433 K, P_{CO}/P_{DME} = 10:1, 20:1, and 50:1.

Figure 10. Respective adsorption density map for the mixture of CO/DME on H-AlMOR and H-AlMOR-Py at 433 K, 0.2 MPa, P_{CO}/P_{DME} = 20:1.

ylation, the reaction mainly occurs in the 8-MR of H-MOR and H-FER. Thus, for the actual reaction situation, H-AlMOR-Py is helpful to improve the adsorption balance and the CO concentration in 8-MR of H-AlMOR.

4. CONCLUSIONS

For the DME carbonylation, pyridine pre-adsorbed hydrogen MOR (H-AlMOR-Py) is beneficial for prolonging the catalyst life. The adsorption and diffusion behaviors of carbonylation on periodic models of H-AlMOR and H-AlMOR-Py were simulated, according to Monte Carlo and molecular dynamics principles.

The adsorption isotherms of the reactants CO and DME on H-AlMOR are quite different: the adsorption amount of CO increases over the whole pressure range; DME adsorption increases rapidly at low pressure but tends to be saturated at high pressure. Thus, the difference makes the molar ratio (N_{CO}/N_{DME}) of the reaction dependent to some extent on CO. The variation trend of pure gases on H-AlMOR-Py with pressure is similar to that on H-AlMOR.

After pyridine pre-adsorption, the adsorption amount of CO decreased by only 22.83%, and the decrease of DME (58.12%) is 2−3 times that of CO. It can be seen that the introduction of pyridine helps to balance the reactant feed ratio.

Table 4. Molar Ratio of CO/DME (N_{CO}/N_{DME}) Adsorbed on H-AlMOR and H-AlMOR-Py at 433 K, 0.2 MPa, P_{CO}/P_{DME} = 10:1, 20:1, 50:1 (Unit: mol/mol)

molecular model	P_{CO}/P_{DME} = 10:1	P_{CO}/P_{DME} = 20:1	P_{CO}/P_{DME} = 50:1
Al-T1O7	0.17	0.30	0.67
Al-T1O7-Py	0.45	0.68	1.41
Al-T2O2	0.17	0.35	0.77
Al-T2O2-Py	0.39	0.67	1.48
Al-T3O1	0.19	0.28	0.75
Al-T3O1-Py	0.46	0.57	1.32
Al-T4O2	0.16	0.31	0.86
Al-T4O2-Py	0.42	0.65	1.42
average value on H-AlMOR	0.17	0.31	0.76
average value on H-AlMOR-Py	0.43	0.64	1.41

The adsorption energy of CO in 8-MR decreased, and the adsorption density of CO in 8-MR was more concentrated on H-AlMOR-Py. Rasmussen[35] et al. showed that 8-MR was the main active site for DME carbonylation, so the introduction of pyridine would also increase the concentration of the reactant CO.

The adsorption amount of product MA decreased by 48.39%, and that of H_2O decreased by 50.88%. The adsorption energy for MA increased by 2.19% in 12-MR, and that of H_2O increased by 11.11−35.71%. The adsorption distribution of DME, MA (in 12-MR), and H_2O significantly decreases. It means product MA and byproduct H_2O are more easily desorbed on H-AlMOR-Py.

After the introduction of pyridine, the self-diffusion coefficient (D_S) decreased to varying degrees. CO (36.54%) and H_2O (35.85%) decrease slightly. DME (40.66%) and MA (75.79%) decrease greatly. The diffusion performance of H-AlMOR-Py is worthy of optimization.

For the mixed feed of DME carbonylation, the feed ratio (P_{CO}/P_{DME}) must reach 50:1 on H-AlMOR so that the reaction molar ratio can reach the theoretical value ($N_{CO}/N_{DME} \approx$ 1:1), while the feed ratio on H-AlMOR-Py is only up to 10:1. Thus, the feed ratio can be adjusted, and raw materials can reduce consumption. In conclusion, H-AlMOR-Py can improve the adsorption equilibrium of reactants CO and DME and increase the concentration of CO in 8-MR.

■ ASSOCIATED CONTENT

Ⓢ Supporting Information

The Supporting Information is available free of charge at https://pubs.acs.org/doi/10.1021/acsomega.3c02127.

Adsorption properties between the H-AlMOR (2 × 1 × 1) model and the H-AlMOR (2 × 2 × 5) model at 433 K and 0.2 MPa (PDF)

■ AUTHOR INFORMATION

Corresponding Author

Haitao Zhang − Engineering Research Centre of Large Scale Reactor Engineering and Technology, Ministry of Education, State Key Laboratory of Chemical Engineering, East China University of Science and Technology, Shanghai 200237, People's Republic of China; Ⓞ orcid.org/0000-0002-1609-0501; Email: zht@ecust.edu.cn

Authors

Jiabao Zhao − Engineering Research Centre of Large Scale Reactor Engineering and Technology, Ministry of Education, State Key Laboratory of Chemical Engineering, East China University of Science and Technology, Shanghai 200237, People's Republic of China; Ⓞ orcid.org/0000-0003-0768-1454

Weixin Qian − Engineering Research Centre of Large Scale Reactor Engineering and Technology, Ministry of Education, State Key Laboratory of Chemical Engineering, East China University of Science and Technology, Shanghai 200237, People's Republic of China; Ⓞ orcid.org/0000-0002-1049-9453

Hongfang Ma − Engineering Research Centre of Large Scale Reactor Engineering and Technology, Ministry of Education, State Key Laboratory of Chemical Engineering, East China University of Science and Technology, Shanghai 200237, People's Republic of China; Ⓞ orcid.org/0000-0002-6752-9019

Weiyong Ying − Engineering Research Centre of Large Scale Reactor Engineering and Technology, Ministry of Education, State Key Laboratory of Chemical Engineering, East China University of Science and Technology, Shanghai 200237, People's Republic of China; Ⓞ orcid.org/0000-0003-3523-6702

Peiqing Yuan − Engineering Research Centre of Large Scale Reactor Engineering and Technology, Ministry of Education, State Key Laboratory of Chemical Engineering, East China University of Science and Technology, Shanghai 200237, People's Republic of China; Ⓞ orcid.org/0000-0003-0797-963X

Complete contact information is available at:
https://pubs.acs.org/10.1021/acsomega.3c02127

Notes

The authors declare no competing financial interest.

■ ACKNOWLEDGMENTS

■ REFERENCES

(1) Zhan, E. S.; Xiong, Z. P.; Shen, W. J. Dimethyl ether carbonylation over zeolites. J. Energy Chem. 2019, 36, 51−63.

(2) Feng, X. B.; Yao, J.; Zeng, Y.; Cui, Y.; Kazumi, S.; Prasert, R.; Liu, G. B.; Wu, J. H.; Yang, G. H.; Tsubaki, N. More efficient ethanol synthesis from dimethyl ether and syngas over the combined nano-sized ZSM-35 zeolite with CuZnAl catalyst. Catal. Today 2021, 369, 88−94.

(3) Lu, P.; Chen, Q. J.; Yang, G. H.; Tan, L.; Feng, X. B.; Yao, J.; Yoneyama, Y.; Tsubaki, N. Space-Confined Self-Regulation Mechanism from a Capsule Catalyst to Realize an Ethanol Direct Synthesis Strategy. ACS Catal. 2020, 10, 1366−1374.

(4) Liu, J. L.; Xue, H. F.; Huang, X. M.; Li, Y.; Shen, W. J. Dimethyl Ether Carbonylation to Methyl Acetate over HZSM-35. Catal. Lett. 2010, 139, 33−37.

(5) Cai, K.; Li, Y.; Shen, H. B.; Cheng, Z. Z.; Huang, S. Y.; Wang, Y.; Ma, X. B. A density functional theory study on the mechanism of

Dimethyl ether carbonylation over heteropolyacids catalyst. *Front. Chem. Sci. Eng.* **2021**, *15*, 319−329.

(6) Cheung, P.; Bhan, A.; Sunley, G. J.; Iglesia, E. Selective carbonylation of dimethyl ether to methyl acetate catalyzed by acidic zeolites. *Angew. Chem., Int. Ed.* **2006**, *45*, 1617−1620.

(7) Bhan, A.; Allian, A. D.; Sunley, G. J.; Law, D. J.; Iglesia, E. Specificity of sites within eight-membered ring zeolite channels for carbonylation of methyls to acetyls. *J. Am. Chem. Soc.* **2007**, *129*, 4919−4924.

(8) Bhan, A.; Iglesia, E. A link between reactivity and local structure in acid catalysis on zeolites. *Acc. Chem. Res.* **2008**, *41*, 559−567.

(9) He, T.; Ren, P. J.; Liu, X. C.; Xu, S. T.; Han, X. W.; Bao, X. H. Direct observation of DME carbonylation in the different channels of H-MOR zeolite by continuous-flow solid-state NMR spectroscopy. *Chem. Commun.* **2015**, *51*, 16868−16870.

(10) Boronat, M.; Martinez-Sanchez, C.; Law, D.; Corma, A. Enzyme-like Specificity in Zeolites: A Unique Site Position in Mordenite for Selective Carbonylation of Methanol and Dimethyl Ether with CO. *J. Am. Chem. Soc.* **2008**, *130*, 16316−16323.

(11) Boronat, M.; Martinez, C.; Corma, A. Mechanistic differences between methanol and dimethyl ether carbonylation in side pockets and large channels of mordenite. *Phys. Chem. Chem. Phys.* **2011**, *13*, 2603−2612.

(12) Cai, K.; Huang, S. Y.; Li, Y.; Cheng, Z. Z.; Lv, J.; Ma, X. B. Influence of Acid Strength on the Reactivity of Dimethyl Ether Carbonylation over H-MOR. *ACS Sustainable Chem. Eng.* **2019**, *7*, 2027−2034.

(13) Wang, X.; Li, R.; Yu, C.; Liu, Y.; Xu, C.; Lu, C. Study on the deactivation process of dimethyl ether carbonylation reaction over Mordenite catalyst. *Fuel* **2021**, *286*, 119480.

(14) Liu, J. L.; Xue, H. F.; Huang, X. M.; Wu, P. H.; Huang, S. J.; Liu, S. B.; Shen, W. J. Stability Enhancement of H-Mordenite in Dimethyl Ether Carbonylation to Methyl Acetate by Pre-adsorption of Pyridine. *Chin. J. Catal.* **2010**, *31*, 729−738.

(15) Rasmussen, D. B.; Christensen, J. M.; Temel, B.; Studt, F.; Moses, P. G.; Rossmeisl, J.; Riisager, A.; Jensen, A. D. Reaction mechanism of dimethyl ether carbonylation to methyl acetate over mordenite a combined DFT/experimental study. *Catal. Sci. Technol.* **2017**, *7*, 1141−1152.

(16) Chen, W.; Li, G. C.; Yi, X. F.; Day, S. J.; Tarach, K. A.; Liu, Z. Q.; Liu, S. B.; Edman Tsang, S. C.; Gora-Marek, K.; Zheng, A. M. Molecular Understanding of the Catalytic Consequence of Ketene Intermediates under Confinement. *J. Am. Chem. Soc.* **2021**, *143*, 15440−15452.

(17) Chen, W.; Tarach, K. A.; Yi, X.; Liu, Z.; Tang, X.; Gora-Marek, K.; Zheng, A. Charge-separation driven mechanism via acylium ion intermediate migration during catalytic carbonylation in mordenite zeolite. *Nat. Commun.* **2022**, *13*, 7106.

(18) Zhao, N.; Tian, Y.; Zhang, L. F.; Cheng, Q. P.; Lyu, S. S.; Ding, T.; Hu, Z. P.; Ma, X. B.; Li, X. G. Spacial hindrance induced recovery of over-poisoned active acid sites in pyridine-modified H-mordenite for dimethyl ether carbonylation. *Chinese Journal of Catalysis* **2019**, *40* (6), 895−904.

(19) Li, Y.; Sun, Q.; Huang, S.; Cheng, Z.; Cai, K.; Lv, J.; Ma, X. Dimethyl ether carbonylation over pyridine-modified MOR: Enhanced stability influenced by acidity. *Catal. Today* **2018**, *311*, 81−88.

(20) Millini, R.; Frigerio, F.; Bellussi, G.; Pazzuconi, G.; Perego, C.; Pollesel, P.; Romano, U. A priori selection of shape-selective zeolite catalysts for the synthesis of 2,6-dimethylnaphthalene. *J. Catal.* **2003**, *217*, 298−309.

(21) Simoncic, P.; Armbruster, T. Peculiarity and defect structure of the natural and synthetic zeolite mordenite: A single-crystal X-ray study. *Am. Mineral.* **2004**, *89*, 421−431.

(22) Akkermans, R. L. C.; Spenley, N. A.; Robertson, S. H. Monte Carlo methods in Materials Studio. *Mol. Simul.* **2013**, *39*, 1153−1164.

(23) Liu, Z. Q.; Yi, X. F.; Wang, G. R.; Tang, X. M.; Li, G. C.; Huang, L.; Zheng, A. M. Roles of 8-ring and 12-ring channels in mordenite for carbonylation reaction: From the perspective of molecular adsorption and diffusion. *J. Catal.* **2019**, *369*, 335−344.

(24) Chibani, S.; Chebbi, M.; Lebegue, S.; Bucko, T.; Badawi, M. A DFT investigation of the adsorption of iodine compounds and water in H-Na-Ag-and Cu- mordenite. *J. Chem. Phys.* **2016**, *144*, 244705.

(25) Jale, S. R.; Bülow, M.; Fitch, F. R.; Perelman, N.; Shen, D. Monte Carlo Simulation of Sorption Equilibria for Nitrogen and Oxygen on LiLSX Zeolite. *J. Phys. Chem. B* **2000**, *104*, 5272−5280.

(26) Akten, E. D.; Siriwardane, R.; Sholl, D. S. Monte Carlo Simulation of Single- and Binary-Component Adsorption of CO2, N2, and H2 in Zeolite Na-4A. *Energy Fuels* **2003**, *17*, 977−983.

(27) Dunne, L. J.; Manos, G.; Du, Z. Exact statistical mechanical one-dimensional lattice model of alkane binary mixture adsorption in zeolites and comparision with Monte-Carlo simulations. *Chem. Phys. Lett.* **2003**, *377*, 551−556.

(28) Zhang, J. F.; Clennell, M. B.; Dewhurst, D. N.; Liu, K. Y. Combined Monte Carlo and molecular dynamics simulation of methane adsorption on dry and moist coal. *Fuel* **2014**, *122*, 186−197.

(29) Sun, H. COMPASS: An ab initio force-field optimized for condensed-phase applications—Overview with details on alkane and benzene compounds. *J. Phys. Chem. B* **1998**, *102*, 7338−7364.

(30) Wu, C.; Xu, W. Atomistic simulation study of absorbed water influence on structure and properties of crosslinked epoxy resin. *Polymer* **2007**, *48*, 5440−5448.

(31) Feng, P.; Zhang, G.; Zang, K.; Li, X.; Xu, L.; Chen, X. A theoretical study on the selective adsorption behavior of dimethyl ether and carbon monoxide on H-FER zeolites. *Chem. Phys. Lett.* **2017**, *684*, 279−284.

(32) Wang, W.; Qian, W.; Ma, H.; Ying, W.; Zhang, H. A theoretical study on the feed ratio of dimethyl ether carbonylation on H-MOR zeolites. *Mol. Phys.* **2021**, *119*, No. e1896044.

(33) He, T.; Liu, X. C.; Xu, S. T.; Han, X. W.; Pan, X. L.; Hou, G. J.; Bao, X. H. Role of 12-Ring Channels of Mordenite in DME Carbonylation Investigated by Solid-State NMR. *J. Phys. Chem. C* **2016**, *120*, 22526−22531.

(34) Zhou, H.; Zhu, W. L.; Shi, L.; Liu, H. C.; Liu, S. P.; Ni, Y. M.; Liu, Y.; He, Y. L.; Xu, S. L.; Li, L. N.; Liu, Z. M. In situ DRIFT study of dimethyl ether carbonylation to methyl acetate on H-mordenite. *J. Mol. Catal. A: Chem.* **2016**, *417*, 1−9.

(35) Rasmussen, D. B.; Christensen, J. M.; Temel, B.; Studt, F.; Moses, P. G.; Rossmeisl, J.; Riisager, A.; Jensen, A. D. Ketene as a Reaction Intermediate in the Carbonylation of Dimethyl Ether to Methyl Acetate over Mordenite. *Angew. Chem., Int. Ed.* **2015**, *54*, 7261−7264.

(36) Cheung, P.; Bhan, A.; Sunley, G. J.; Law, D. J.; Iglesia, E. Site requirements and elementary steps in dimethyl ether carbonylation catalyzed by acidic zeolites. *J. Catal.* **2007**, *245*, 110−123.